

Electrical Breakdown of Excitonic Insulator

Yuelin Shao^{1,2,*} and Xi Dai^{3,†}

¹*Beijing National Laboratory for Condensed Matter Physics and Institute of Physics,
Chinese Academy of Sciences, Beijing 100190, China*

²*School of Physical Sciences, University of Chinese Academy of Sciences, Beijing 100049, China*

³*Department of Physics, The Hongkong University of Science and Technology,
Clear Water Bay, Kowloon 999077, Hong Kong, China*

(Dated: February 16, 2023)

The intrinsic electrical breakdown of normal insulators is usually attributed to inter-band Zener tunneling. This occurs when the gate voltage reaches the same level as the bandgap. As a result, the Zener critical field is inversely proportional to the size of the system. However, when the electric field is strong enough to disrupt excitons, an excitonic insulator will also break down, as its insulation is due to the pairing of free electrons and holes. Unlike the Zener mechanism, the pair-breaking critical field has little dependence on system size and has a finite value in the thermodynamic limit. To understand the relationship between these two mechanisms, a Hartree Fock calculation that takes into account polarization was performed on a 2D bilayer model. Phase diagrams were generated as a function of electric field, system size, and exciton density. The results showed that, at the large scale (low exciton density) limit, the breakdown is dominated by Zener tunneling and transitions smoothly to the pair-breaking case as the system size decreases (exciton density increases). This provides a straightforward way to distinguish excitonic insulators from normal insulators.

I. INTRODUCTION

The excitonic insulator is an insulating phase where electron-hole pairs condensate[1–4]. In semiconductors, this phase appears when the binding energy of excitons exceeds the band gap, as the spontaneous generation and condensation of excitons lead to a lowering of the system's energy. On the other hand, in semimetals, where the Fermi surfaces for electrons and holes are comparable, the attractive Coulomb interaction binds the free electrons and holes. This BCS-like condensation in momentum space near the Fermi surface opens an energy gap and results in an excitonic insulating state.

The short lifetime of excitons in semiconductors often impedes the realization of exciton condensation. To overcome this challenge, indirect excitons in bilayer systems such as quantum wells or van der Waals heterostructures are often used[5–7]. The real space separation of electrons and holes in these systems results in a longer lifetime for excitons, and the weak screening in 2D makes it easier for the binding to occur. So far, a large body of experimental[8–13] and theoretical[14–18] studies have been conducted to investigate the properties of excitonic insulators in such 2D bilayer systems.

Recently, electrical breakdown measurements in transport experiments have revealed that excitonic insulators tend to break down more easily than normal insulators[19]. This observation is in agreement with the theoretical conclusion that the threshold electric field required to induce electrical breakdown in a correlated insulator is much weaker than the Zener breakdown threshold in a normal band insulator [20]. However, the inter-

play between the interaction and Zener breakdown in excitonic insulators is not yet fully understood and requires further study.

Let's illustrate the breakdown of excitonic insulators by a 2D bilayer system with a non-zero inter-layer distance, as shown in Fig. 1(a). The application of a vertical displacement field \mathcal{E}_\perp will result in the charging of the two layers by electrons and holes. If the interaction is absent, the charged bilayer would be expected to exhibit metallic behavior. However, the presence of an attractive interaction $U(r)$ between electrons and holes will drive the system into an excitonic insulator state at the charge neutral point (CNP). When an in-plane electric field \mathcal{E} is gradually added, the excitonic insulator is expected to polarize and eventually break down.

The most well-known intrinsic mechanism for electrical breakdown is inter-band Zener tunneling as shown in Fig. 1(b). In an infinite insulating system, the total energy becomes unbounded when an electric field is applied, resulting in the absence of a ground state. However, a finite system can still maintain an insulating stationary state at low electric fields [21, 22]. When the gate voltage becomes comparable to the bandgap, i.e. $e\mathcal{E}L \sim \Delta$, this stationary state disappears, leading to the so-called inter-band Zener breakdown[23–25]. This means that the Zener critical field \mathcal{E}_c^z is inversely proportional to the size of the system

$$e\mathcal{E}_c^z(L)/\Delta \sim L^{-1}. \quad (1)$$

While inter-band Zener breakdown occurs in any band-insulating system in the thermodynamic limit, there is another breakdown mechanism unique to excitonic insulators. In the BCS limit, the insulation of an excitonic insulator is derived from the pairing of free electrons and holes. When the external electric field becomes strong

* ylshao@iphy.ac.cn

† daix@ust.hk

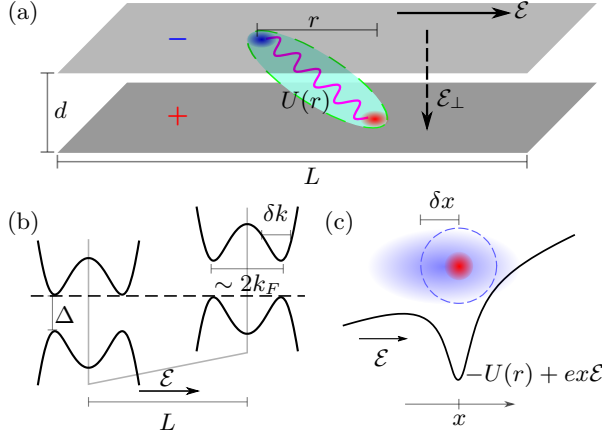


FIG. 1. (a) Setup of the bilayer system. A vertical displacement field \mathcal{E}_\perp is used to charge the two layers with electrons and holes. At the charge neutral point, attractive interaction $U(r)$ between electrons and holes will drive the system into an excitonic insulator phase. When an in-plane electric field \mathcal{E} is applied, the insulating system will polarize and even break down. (b) Exciton condensation happens mainly near the Fermi surface in the range $k_F \pm \delta k/2$ which generates an excitonic gap Δ . Inter-band Zener breakdown happens when the gate voltage is comparable to the band gap, i.e. $e\mathcal{E}L \sim \Delta$. (c) In real space, an excitonic insulator could be viewed as the condensation of weakly bound electron-hole pairs with radius $r_{ex} = 2\pi/\delta k$. With the increase of electric field strength, the barrier for the electron to escape the trap of the hole gets lower and lower. The electron will eventually escape the trap and pair breaking occurs.

enough to disrupt these excitonic pairs, the insulation property is also lost and a transition from an insulating state to a conductive state occurs.

The condensation in momentum space happens around the Fermi surface within the range $k_F \pm \delta k/2$, where $k_F = \sqrt{4\pi n_{ex}}$ is Fermi vector and momentum uncertainty δk is about Δ/v_F . Then the radius of an exciton could be evaluated by uncertainty principle as $r_{ex} \sim \delta x \sim 2\pi/\delta k = 2\pi v_F/\Delta$. An external electric field will tilt the electrical potential around the hole and polarize the exciton. The exciton pair-breaking occurs when the distribution of electrons crosses the potential barrier, and the hole can't trap the electron anymore, as illustrated in Fig.1(c). This ionization process is localized in real space and insensitive to system scale when the system scale L is much larger than the exciton size r_{ex} . So the pair-breaking field should be finite in the thermodynamic limit, and the scale dependence of pair breaking field takes the form

$$e\mathcal{E}_c^{ex}(L)/\Delta \sim e\mathcal{E}_c^{ex}(\infty)/\Delta + \alpha L^{-1} + O(L^{-2}), \quad (2)$$

which is quite different from Eq. (1).

II. POLARIZATION MEAN FIELD THEORY

The actual breakdown scenario in an excitonic insulator is complex, as reaching either of the two critical fields Eq. (1)(2) results in the electrical breakdown. To better understand the breakdown of excitonic insulators, we will utilize a self-consistent mean field theory to analyze the interplay between these two mechanisms.

For simplicity, we will limit our analysis to the conduction band in the electron layer and the highest valence band in the hole layer. These bands can be described by the electron creation operators $c_{e\mathbf{k}}^\dagger$ and $c_{h\mathbf{k}}^\dagger$, respectively.

Within the $k \cdot p$ approximation, the many-body Hamiltonian can be written as

$$H = \sum_{s=e,h\mathbf{k}} h_{ss'\mathbf{k}}^0 c_{s\mathbf{k}}^\dagger c_{s'\mathbf{k}} + e\mathcal{E} \cdot \int d\mathbf{r} \Psi^\dagger(\mathbf{r}) \mathbf{r} \Psi(\mathbf{r}) + \frac{1}{2\mathcal{V}} \sum_{ss'=e,h\mathbf{k}_1\mathbf{k}_2\mathbf{q}} V_{ss'}(\mathbf{q}) c_{s\mathbf{k}_1}^\dagger c_{s'\mathbf{k}_2}^\dagger c_{s'\mathbf{k}_2+\mathbf{q}} c_{s\mathbf{k}_1-\mathbf{q}}, \quad (3)$$

where \mathcal{V} is the area of the 2D system and $\Psi(\mathbf{r})$ is field operator defined as $\Psi(\mathbf{r}) = \mathcal{V}^{-1/2} \sum_{s\mathbf{k}} e^{i\mathbf{k} \cdot \mathbf{r}} u_s(\mathbf{r}) c_{s\mathbf{k}}$.

The single particle Hamiltonian $h_{\mathbf{k}}^0$ can be taken as

$$h_{\mathbf{k}}^0 = \begin{bmatrix} k^2/2m_e - \mu_e & 0 \\ 0 & -k^2/2m_h + \mu_h \end{bmatrix}. \quad (4)$$

where $m_{e,h}$ are effective masses of these two kind of electrons and $\mu_{e,h}$ are chemical potentials tuned by displacement field \mathcal{E}_\perp . Vanishing of the off-diagonal term in Eq. (4) means direct inter-layer hopping is forbidden. This assumption is made because we are concerned with the breakdown of an excitonic gap. In real materials, this could be realized by symmetry constraints or just a large separation between layers. The inter- and intra-layer interaction are taken as the Coulomb ones: $V(r) \equiv V_{s=s'} = e^2/\epsilon r$ and $U(r) \equiv V_{s \neq s'} = e^2/\epsilon \sqrt{r^2 + d^2}$ whose Fourier transformations are $V(q) = 2\pi e^2/\epsilon q$, $U(q) = V(q)e^{-qd}$.

Even under an in-plane field breaks translation symmetry, for an insulating ground state, we can always take a trial Hartree-Fock(HF) ground state that keeps translation symmetry as long as the field is adiabatically added (The proof is in Appendix A). A trial HF state at CNP is $|G\rangle = \prod_{\mathbf{k}} c_{v\mathbf{k}}^\dagger |\text{vac.}\rangle$ where the valance band $c_{v\mathbf{k}}^\dagger = \alpha_{\mathbf{k}} c_{e\mathbf{k}}^\dagger + \beta_{\mathbf{k}} c_{h\mathbf{k}}^\dagger$ is a linear combination of the electron and hole band with constraints $|\alpha|^2 + |\beta|^2 = 1$. By using Dirac notation $|v\mathbf{k}\rangle = [\alpha_{\mathbf{k}}, \beta_{\mathbf{k}}]^T$, energy difference per area between HF ground state $|G\rangle$ and the uncharged state $|G_0\rangle = \prod_{\mathbf{k}} c_{h\mathbf{k}}^\dagger |\text{vac.}\rangle$ becomes a functional of $|v\mathbf{k}\rangle$

(a general derivation could be found in Appendix B)

$$\begin{aligned}
& \varepsilon_{tot}[\langle v\mathbf{k} \rangle; \mathcal{E}] \\
& \equiv \frac{1}{\mathcal{V}} \langle G | H | G \rangle - \frac{1}{\mathcal{V}} \langle G_0 | H | G_0 \rangle \\
& = \frac{1}{\mathcal{V}} \sum_{s\mathbf{k}} h_{ss\mathbf{k}}^0 \tilde{\rho}_{ss\mathbf{k}} + \frac{-e\mathcal{E}}{\mathcal{V}\Delta k_{\parallel}} \text{Im} \sum_{\mathbf{k}_{\perp}} \log \prod_{\mathbf{k}_{\parallel}} \langle v\mathbf{k} | v\mathbf{k} + \Delta\mathbf{k}_{\parallel} \rangle \\
& \quad + \frac{2\pi e^2 n_{ex}^2 d}{\epsilon} - \frac{1}{2\mathcal{V}^2} \sum_{ss'\mathbf{k}_1\mathbf{k}_2} V_{ss'}(\mathbf{k}_1 - \mathbf{k}_2) \tilde{\rho}_{ss'\mathbf{k}_1} \tilde{\rho}_{s'\mathbf{k}_2},
\end{aligned} \tag{5}$$

where $\tilde{\rho} \equiv \rho - \rho^0$ is the density matrix relative to the initial uncharged state $\rho_{ss'}^0 = \delta_{ss'}\delta_{sh}$ and ρ is calculated as $\rho_{ss'\mathbf{k}} = \langle G | c_{s'\mathbf{k}}^\dagger c_{s\mathbf{k}} | G \rangle = (\langle v\mathbf{k} | \langle v\mathbf{k} \rangle)_{ss'}$.

The four terms in Eq. (5) could be viewed as kinetic, polarization, Hartree, and Fock energies separately. Hartree energy is just the charging energy of the two-layer capacitor with the electron/hole number density (exciton density) $n_{ex} = 1/\mathcal{V} \sum_{\mathbf{k}} \rho_{ee\mathbf{k}}$. The relative density matrix $\tilde{\rho}$ is used in the Fock energy expression to avoid double counting problems[14]. For numerical convenience, a periodic boundary condition is assumed, and the polarization energy is calculated with the help of the expectation value of many-body position operators defined on a ring geometry[26], which is just a discrete form of Berry phase [27–29]. This form of polarization energy functional has already been used to calculate the electrical properties of insulators in the literature[22, 30, 31]. On the other hand, for the open boundary problem, the polarization energy functional should be written in real space by Wannier functions[32, 33] which can be more complex.

The local minimum is found by requiring the first order derivative of ε_{tot} to be zero, i.e. $\delta\varepsilon_{tot}/\delta\langle v\mathbf{k} \rangle = 0$. This gives the mean field Hamiltonian $h_{\mathbf{k}}^{MF} \equiv h_{\mathbf{k}}^0 + h_{\mathbf{k}}^H + h_{\mathbf{k}}^F + h_{\mathbf{k}}^P$ where

$$h_{\mathbf{k}}^H[\langle v\mathbf{k} \rangle] = \frac{4\pi e^2 n_{ex} d}{\epsilon} (1 - \rho^0), \tag{6a}$$

$$h_{ss'\mathbf{k}}^F[\langle v\mathbf{k} \rangle] = -\frac{1}{\mathcal{V}} \sum_{\mathbf{k}'} V_{s's}(\mathbf{k} - \mathbf{k}') \tilde{\rho}_{ss'\mathbf{k}'}, \tag{6b}$$

$$h_{\mathbf{k}}^P[\langle v\mathbf{k} \rangle; \mathcal{E}] = \frac{ie\mathcal{E}}{2\Delta k_{\parallel}} \sum_{\sigma=\pm} \frac{\sigma \langle v\mathbf{k} + \sigma\Delta\mathbf{k}_{\parallel} | \langle v\mathbf{k} \rangle}{\langle v\mathbf{k} | v\mathbf{k} + \sigma\Delta\mathbf{k}_{\parallel} \rangle} + h.c., \tag{6c}$$

as well as the self-consistent equation

$$h_{\mathbf{k}}^{MF}[\langle v\mathbf{k} \rangle; \mathcal{E}] | v\mathbf{k} \rangle = \xi_{v\mathbf{k}} | v\mathbf{k} \rangle. \tag{7}$$

A general derivation can be found in Appendix C.

III. RESULTS

In the phase diagram depicted in Fig. 2, the x -axis is scaled by $1/L_x$ and the y -axis represents the normalized electric field, $e\mathcal{E}/\Delta^0$. The electric field is normalized by

the zero field band gap, Δ^0 , as the band gap is also scale-dependent, as shown in the inset of Fig. 2.

The length scale L is defined by the spacing of k -mesh as $L = 2\pi/\Delta k$. We use a unified momentum space cut-off $|k_{x,y}| < k_c = 0.05 \text{ a.u.} \approx 0.094 \text{ \AA}^{-1}$ (encloses an area about $1/10^2$ the Brillouin zones of general TMD materials), so the varying of length scale can be realized by using different sizes of k -mesh. The number of k points in y direction is fixed as $N_{k_y} = 40$ and $L_y \approx 133 \text{ nm}$. While in x direction (the direction of electric field), the number of k points N_{k_x} is taken from $N_{k_x} \in [160, 1600]$, which gives a length scale L_x varies from 533 nm to 5333 nm . The corresponding N_{k_x} s are marked above the bottom axis in Fig. 2 with red text. The number of excitons in the corresponding length scale is also marked on the top axis for reference.

The other parameters are set as $m_{e,h} = 0.3m_0$ (m_0 is the electron bare mass), $\epsilon = 7$ and $d = 80 \text{ a.u.} \approx 44 \text{ \AA}$. The chemical potentials are fixed at $\mu_e = \mu_h = 8 \times 10^{-4} \text{ a.u.} \approx 22 \text{ meV}$ which charge these two layers with electron/hole densities to about 10^{-4} \AA^{-2} (varied with scale as shown in the inset of Fig. 2).

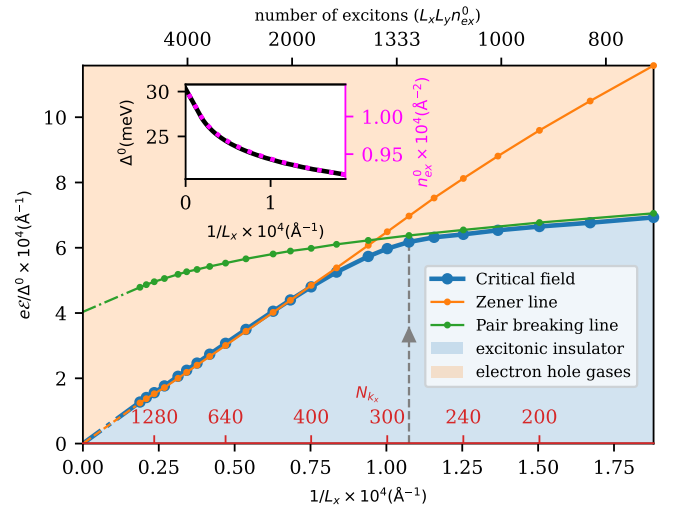


FIG. 2. Phase diagram as a function of length scale $1/L_x$ and electric field $e\mathcal{E}/\Delta^0$ (normalized by zero field band gap Δ^0). The critical field divides the entire region into the excitonic insulator and the electron-hole gas phase. The Zener line is the critical field for a hard gap insulator while the pair-breaking line is for an excitonic insulator with suppressed Zener tunneling. The dashed parts of these lines in the large-scale limit are extrapolations. The red labels above the bottom axis mark the number of k points used for the corresponding length scales and the top axis represents the number of excitons in such a scale. In the inset, zero field band gap Δ^0 (black solid line, left axis) and zero field exciton density n_{ex}^0 (purple dashed line, right axis) are also plotted as functions of $1/L_x$ for reference.

The blue line in Fig. 2(a) is the critical field of electrical breakdown predicted by our theory, which divides the entire region into the excitonic insulator phase and

the electron-hole gas phase. The orange Zener line is obtained by treating the soft excitonic gap as a hard one, i.e. the Hartree and Fock Hamiltonians are fixed to be the unpolarized ones $h_{\mathbf{k}}^{HF}(\mathcal{E} = 0)$ and don't get updated during the self-consistent procedure. Then a Zener tunneling behavior described by Eq. (1) is observed in the entire length scale range. To get the green pair breaking line, a series of $40M \times 40$ ($4 \leq M \leq 40$) k -meshes are used while the polarization Hamiltonian $h_{\mathbf{k}}^P$ and the polarization energy E_P are always evaluated on the coarse 40×40 mesh to avoid inter-band Zener tunneling. The finite intercept of this line implies a nonzero pair breaking field \mathcal{E}_c^{ex} in thermodynamic limit. Therefore, a critical scale where the Zener and pair-breaking lines intersect could be estimated as

$$L_c \sim \Delta / e\mathcal{E}_c^{ex}. \quad (8)$$

In large scale limit ($L \gg L_c$), the breaking down of an excitonic insulator is Zener-like, while a pair-breaking behavior presents in small scale ($L \ll L_c$).

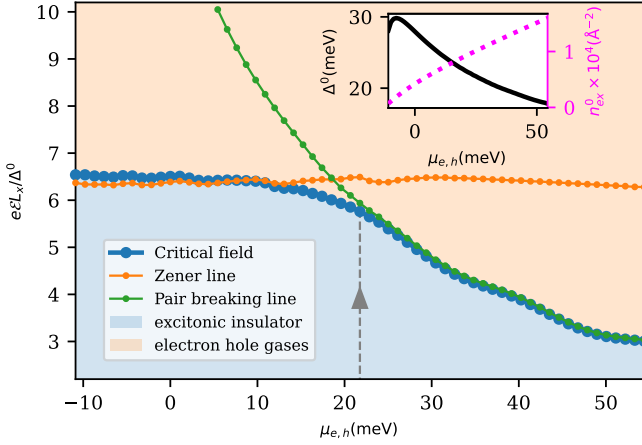


FIG. 3. Phase diagram as a function of chemical potential $\mu_e (= \mu_h)$ and electric field strength $e\mathcal{E}L_x/\Delta^0$ (normalized by zero field band gap Δ^0 and length scale L_x). To get this plot, a fixed 280×40 k -mesh is used while the chemical potentials for electrons and holes are set equal and vary from -10 meV to 55 meV. The physical meanings of the different regions and lines are the same as that in Fig. 2. The inset shows zero field band gaps and exciton densities as functions of chemical potentials for reference.

This crossover also happens with the change of exciton density (or chemical potentials). To see this, the phase diagram as a function of chemical potentials $\mu_e (= \mu_h)$ and electric field $e\mathcal{E}L_x/\Delta^0$ is also shown in Fig. 3. The length scale is fixed (k -mesh is fixed at 280×40) and the chemical potentials $\mu_{e,h}$ vary to change the exciton density. Using the same methods as before, the critical field, Zener, and pair-breaking lines are generated. It's easy to see that at low exciton densities, the pair-breaking field is much larger than the Zener field and the breakdown of an excitonic insulator is Zener-like. As exciton density increases, exciton pairing becomes weaker. The

pair-breaking field decreases and eventually takes over the breakdown behaviors.

To understand the breakdown phase transition, let's examine the stability of the local minimum, which is realized by calculating the second-order derivatives (Hessian matrix) of the energy functional.

Assume we are in the region of insulating state, so the local minimum $|v\mathbf{k}; \mathcal{E}\rangle$ could be found by our self-consistent procedure. The self-consistent equation at the mean field solution reads $h_{\mathbf{k}}^{MF}[|v\mathbf{k}; \mathcal{E}\rangle; \mathcal{E}]|i\mathbf{k}; \mathcal{E}\rangle = \xi_{i\mathbf{k}, \mathcal{E}}|i\mathbf{k}; \mathcal{E}\rangle$, where $|c\mathbf{k}; \mathcal{E}\rangle, |v\mathbf{k}; \mathcal{E}\rangle$ are conduction and valance bands with band energies $\xi_{c\mathbf{k}, \mathcal{E}} > \xi_{v\mathbf{k}, \mathcal{E}}$. At the local minimum, the trial HF state could be reparameterized as

$$|v'\mathbf{k}; \mathcal{E}\rangle = (|v\mathbf{k}; \mathcal{E}\rangle + f_{\mathbf{k}}|c\mathbf{k}; \mathcal{E}\rangle)/\sqrt{1 + |f_{\mathbf{k}}|^2}. \quad (9)$$

This parametrization is complete and unconstrained ($f_{\mathbf{k}}$ is an arbitrary complex-valued function). Then the total energy becomes a functional of $f_{\mathbf{k}}$, i.e. $\varepsilon_{tot}[f_{\mathbf{k}}, f_{\mathbf{k}}^*; \mathcal{E}] \equiv \varepsilon_{tot}[|v'\mathbf{k}; \mathcal{E}\rangle; \mathcal{E}]$, and the Hessian matrix at this point is

$$H_{\mathbf{k}\mathbf{k}'} = \begin{pmatrix} \frac{\delta \varepsilon_{tot}}{\delta \text{Re} f_{\mathbf{k}} \delta \text{Re} f_{\mathbf{k}'}} & \frac{\delta \varepsilon_{tot}}{\delta \text{Re} f_{\mathbf{k}} \delta \text{Im} f_{\mathbf{k}'}} \\ \frac{\delta \varepsilon_{tot}}{\delta \text{Im} f_{\mathbf{k}} \delta \text{Re} f_{\mathbf{k}'}} & \frac{\delta \varepsilon_{tot}}{\delta \text{Im} f_{\mathbf{k}} \delta \text{Im} f_{\mathbf{k}'}} \end{pmatrix} \bigg|_{f_{\mathbf{k}}=0}. \quad (10)$$

The details and specific expression of $H_{\mathbf{k}\mathbf{k}'}$ could be found in Appendix D.

If $f_{\mathbf{k}}$ is small, $|v'\mathbf{k}; \mathcal{E}\rangle$ is approximated by $|v'\mathbf{k}; \mathcal{E}\rangle \sim |v\mathbf{k}; \mathcal{E}\rangle + f_{\mathbf{k}}|c\mathbf{k}; \mathcal{E}\rangle$. Such a form can be viewed as the low-energy excitation modes in the variational parameter space illustrated above. By diagonalizing the Hessian matrix, the eigenmodes for the low-energy excitations $\sum_{\mathbf{k}'} H_{\mathbf{k}\mathbf{k}'} f_{\mathbf{k}'}^\lambda = \lambda f_{\mathbf{k}}^\lambda$ can be obtained. For convenience, the eigenmodes in the following text are normalized by $f_{\mathbf{k}}^\lambda \rightarrow f_{\mathbf{k}}^\lambda / \sqrt{\sum_{\mathbf{k}} |f_{\mathbf{k}}^\lambda|^2}$.

On a 280×40 k -mesh with chemical potentials $\mu_{e,h} = 8 \times 10^{-4}$ a.u. (dashed gray arrow line in Fig. 2 and Fig. 3), the total energy functional is analyzed, and the results are shown in Fig. 4. In Fig. 4(a), we plot the smallest few eigenvalues λ_{0-4} of the Hessian matrix Eq. (10) as functions of field strength. By taking trial HF states as $|v'\mathbf{k}; \mathcal{E}; \theta_{\lambda_i}\rangle \propto |v\mathbf{k}; \mathcal{E}\rangle + \theta_{\lambda_i} f_{\mathbf{k}}^{\lambda_i} |c\mathbf{k}; \mathcal{E}\rangle$, the total energy along these directions $f_{\mathbf{k}}^{\lambda_i}$ in configuration space are evaluated as

$$\Delta \varepsilon_{tot}(\mathcal{E}, \theta_{\lambda_i}) \equiv \varepsilon_{tot}[|v'\mathbf{k}; \mathcal{E}; \theta_{\lambda_i}\rangle] - \varepsilon_{tot}[|v\mathbf{k}; \mathcal{E}\rangle]. \quad (11)$$

Using the lowest three eigenmodes $f_{\mathbf{k}}^{\lambda_{0,1,2}}$ for example, the total energy as the function of the electric field \mathcal{E} and excitation amplitudes θ_{λ_i} are plotted in Fig. 4(b)(c)(d). In these plots, the horizontal axes are the amplitudes of those eigenmodes along the directions $f_{\mathbf{k}}^{\lambda_i}$ in parameter space, while different electric field strengths are represented by different color lines.

There is a consistent zero mode λ_0 for any finite electric field strength, as shown in Fig. 4(a). However, the behaviors of the total energy functional along the direction $f_{\mathbf{k}}^{\lambda_0}$ in Fig. 4(b) indicates that it's not a "breaking down

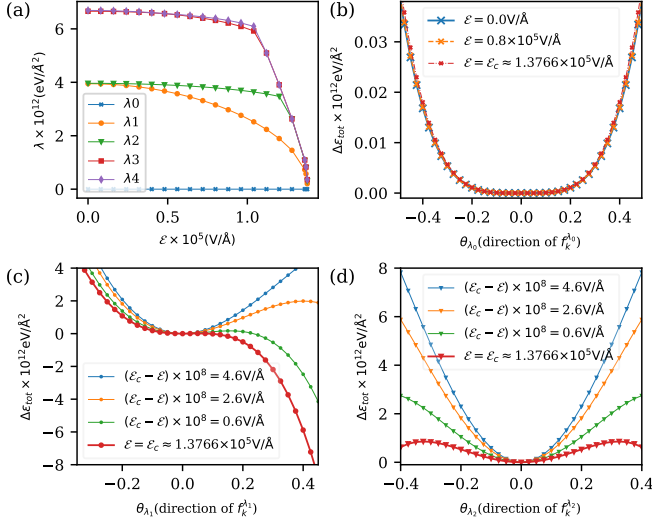


FIG. 4. (a) The smallest five eigenvalues of the Hessian matrix Eq. (10) as a function of the electric field. (b)(c)(d) Total energy as a function of the electric field and excitation amplitudes along the directions of $f_k^{\lambda_{0,1,2}}$ in configuration space. The excitation amplitudes are used as the horizontal axes while different field strengths are represented by different color lines. These data are generated on a 280×40 k -mesh with chemical potentials fixed at $\mu_{e,h} = 8 \times 10^{-4}$ a.u. (along the dashed gray arrow line in Fig. 2 and Fig. 3).

mode” because the high-order derivatives of the total energy functional along this direction are always positive. Such a zero mode is the Goldstone mode related to phase fluctuation of the electron-hole pairing condensate $\rho_{eh\mathbf{k}}$ as discussed in Appendix E.

The real breaking down direction in parameter space is $f_k^{\lambda_1}$ as shown in Fig. 4(c). When the electric field is small, all eigenvalues of the Hessian matrix (except the Goldstone mode λ_0) satisfy $\lambda > \lambda_1 > 0$, which means the solution is indeed a local minimum. As the electric field approaches the critical field strength \mathcal{E}_c , the eigenvalue of the breakdown mode λ_1 approaches 0 and the excitonic insulator ground state becomes unstable as the local minimum turns into a saddle point. In contrast, the energy barrier along the other directions, such as $f_k^{\lambda_2}$ shown in Fig. 4(d), also decreases with increasing electric field strength but remains positive even at the critical field strength.

IV. DISCUSSION

Although the calculation is conducted on a simple model, we believe the scale dependence of these two breakdown mechanisms, Zener tunneling Eq. (1) and pair-breaking Eq. (2) are universal. Thus a crossover of the critical field from the pair-breaking region to the Zener tunneling region should be observed with the increase in scale. And a critical scale L_c where the crossover happens could be defined for such an excitonic insulating

system.

If the critical scale is too small to hold any exciton (for example, atomic scale), this so-called “excitonic insulator” is indistinguishable from the normal one from the perspective of electrical breakdown. Only when the critical scale is large enough the insulating gap might exhibit its excitonic properties in an electric field.

In realistic experiments, the scale is fixed but the exciton density could be tuned by the displacement field. At the BEC limit with low exciton density, the electron and hole are tightly bound, so the pair-breaking field is expected to be very large and the breaking down is dominated by Zener tunneling. For the same system, the critical field for Zener tunneling $e\mathcal{E}_c^z L/\Delta$ is expected to be insensitive to the change of exciton density. However, the binding between electron and hole is very sensitive and the pair-breaking field $e\mathcal{E}_c^{ex} L/\Delta$ decreases rapidly with the increase of exciton density. When \mathcal{E}_c^z is much bigger than \mathcal{E}_c^{ex} at a high exciton density limit, the pair-breaking mechanism will eventually take over the electrical breaking down behaviors.

At last, the scale in our calculation should be understood as the smaller one of the actual size of a real system and its coherence length. Above the coherence length, the system is just a series circuit. And the entire system breaks down only when all the subsystems are broken down. So the actual critical field should be chosen as the largest among the critical fields of all the sub-systems.

Appendix A: The Trial State

We first prove that under a uniform electric field, the many-body state will keep its lattice translation symmetry at all times.

A many-body state $|\Psi; t\rangle$ is said to have lattice translation symmetry if and only if the wavefunction satisfies

$$\Psi(\mathbf{r}_1, +\mathbf{R}_0, \dots, \mathbf{r}_{N_e} + \mathbf{R}_0; t) = e^{i\phi} \Psi(\mathbf{r}_1, \dots, \mathbf{r}_{N_e}; t),$$

where N_e is the total number of electrons and \mathbf{R}_0 is arbitrary lattice vector.

The many-body Schrödinger equation in length gauge (using a scalar field $\varphi = e\mathcal{E} \cdot \mathbf{r}$ to include electric field) is written as

$$i\partial_t \Psi^E(\mathbf{r}_1, \dots, \mathbf{r}_{N_e}; t) = \left\{ \sum_{i=1}^{N_e} [h^0(-i\nabla_{\mathbf{r}_i}, \mathbf{r}_i) + e\mathcal{E} \cdot \mathbf{r}_i] + \sum_{1 \leq i < j \leq N_e} V(\mathbf{r}_i - \mathbf{r}_j) \right\} \Psi^E(\mathbf{r}_1, \dots, \mathbf{r}_{N_e}; t), \quad (\text{A1})$$

which seems to break lattice translation symmetry. However, by taking gauge transformation of the electric field $\partial_t \mathbf{A}(t) = -\mathcal{E}$ and defining

$$\Psi^A(\mathbf{r}_1, \dots, \mathbf{r}_{N_e}; t) = e^{-i \sum_{i=1}^{N_e} e\mathbf{A}(t) \cdot \mathbf{r}_i} \Psi^E(\mathbf{r}_1, \dots, \mathbf{r}_{N_e}; t), \quad (\text{A2})$$

we find that the Schrödinger equation for $|\Psi^A\rangle$ becomes

$$i\partial_t \Psi^A(\mathbf{r}_1, \dots, \mathbf{r}_{N_e}; t) = \left[\sum_{i=1}^{N_e} h^0(-i\nabla_{\mathbf{r}_i} + e\mathbf{A}(t), \mathbf{r}_i) + \sum_{1 \leq i < j \leq N_e} V(\mathbf{r}_i - \mathbf{r}_j) \right] \Psi^A(\mathbf{r}_1, \dots, \mathbf{r}_{N_e}; t), \quad (\text{A3})$$

which keeps the lattice translation symmetry. So starting from a many-body state $|\Psi^0\rangle$ with lattice translation symmetry, the many-body state $|\Psi^A; t\rangle$ as well as $|\Psi^E; t\rangle$ will have lattice translation symmetry at any time:

$$\begin{aligned} & \Psi^E(\mathbf{r}_1 + \mathbf{R}_0, \dots, \mathbf{r}_{N_e} + \mathbf{R}_0; t) \\ &= e^{i \sum_{i=1}^{N_e} e\mathbf{A}(t) \cdot (\mathbf{r}_i + \mathbf{R}_0)} \Psi^A(\mathbf{r}_1 + \mathbf{R}_0, \dots, \mathbf{r}_{N_e} + \mathbf{R}_0; t) \\ &= e^{iN_e e\mathbf{A}(t) \cdot \mathbf{R}_0 + i\phi_A} e^{i \sum_{i=1}^{N_e} \mathbf{A}(t) \cdot \mathbf{r}_i} \Psi^A(\mathbf{r}_1, \dots, \mathbf{r}_{N_e}; t) \\ &= e^{iN_e e\mathbf{A}(t) \cdot \mathbf{R}_0 + i\phi_A} \Psi^E(\mathbf{r}_1, \dots, \mathbf{r}_{N_e}; t). \end{aligned} \quad (\text{A4})$$

When treating a static uniform electric field, as long as the field is adiabatically turned on, a trial HF state with lattice translation symmetry could be safely assumed. For insulators, this state is written as

$$|GS\rangle = \prod_{n=1}^{n_e} \prod_{\mathbf{k} \in BZ} c_{n\mathbf{k}}^\dagger |\text{vac.}\rangle, \quad (\text{A5})$$

where n_e is electron per cell and $|\text{vac.}\rangle$ is vacuum state. $c_{n\mathbf{k}}^\dagger$ is creation operators of Bloch electron with wavefunction

$$\psi_{n\mathbf{k}}(\mathbf{r}) = \{\Psi(\mathbf{r}), c_{n\mathbf{k}}^\dagger\} = \frac{1}{\sqrt{\mathcal{V}}} e^{i\mathbf{k} \cdot \mathbf{r}} u_{n\mathbf{k}}(\mathbf{r}), \quad (\text{A6})$$

where $\mathcal{V} = \mathcal{N}v_c$ is the volume of the system, \mathcal{N} is the number of unit cells and v_c is cell volume.

As electron creation operators, $c_{n\mathbf{k}}^\dagger$ should satisfy

$$\{c_{m\mathbf{k}}^\dagger, c_{n\mathbf{k}'}\} = \delta_{mn} \delta_{\mathbf{k}\mathbf{k}'}, \quad (\text{A7})$$

which forces the corresponding Bloch functions to be orthonormal, i.e.

$$\langle \psi_{m\mathbf{k}} | \psi_{n\mathbf{k}'} \rangle = \int d\mathbf{r} \psi_{m\mathbf{k}}^*(\mathbf{r}) \psi_{n\mathbf{k}'}(\mathbf{r}) = \delta_{mn} \delta_{\mathbf{k}\mathbf{k}'}, \quad (\text{A8a})$$

$$\langle u_{m\mathbf{k}} | u_{n\mathbf{k}} \rangle = \frac{1}{v_c} \int_{\text{cell}} d\mathbf{r} u_{m\mathbf{k}}^*(\mathbf{r}) u_{n\mathbf{k}}(\mathbf{r}) = \delta_{mn}. \quad (\text{A8b})$$

Appendix B: Polarization HF Energy Functional

In this part, a general form of the polarization Hartree Fock energy as a functional of occupied Bloch states will be derived.

Using field operator $\Psi(\mathbf{r})$, the second quantization form of single particle (kinetic and potential energy), po-

larization, and interaction Hamiltonians are written as

$$H_0 = \int d\mathbf{r} \Psi^\dagger(\mathbf{r}) h^0(-i\nabla_{\mathbf{r}}, \mathbf{r}) \Psi(\mathbf{r}), \quad (\text{B1})$$

$$H_P = e\mathcal{E} \cdot \int d\mathbf{r} \Psi^\dagger(\mathbf{r}) \mathbf{r} \Psi(\mathbf{r}), \quad (\text{B2})$$

$$H_I = \frac{1}{2} \int d\mathbf{r}_1 d\mathbf{r}_2 \Psi^\dagger(\mathbf{r}_1) \Psi^\dagger(\mathbf{r}_2) V(\mathbf{r}_1 - \mathbf{r}_2) \Psi(\mathbf{r}_2) \Psi(\mathbf{r}_1). \quad (\text{B3})$$

The single-particle correlation function is calculated as

$$\begin{aligned} \rho(\mathbf{r}, \mathbf{r}') &\equiv \langle GS | \Psi^\dagger(\mathbf{r}') \Psi(\mathbf{r}) | GS \rangle \\ &= \sum_{n=1}^{n_e} \sum_{\mathbf{k} \in BZ} \{c_{n\mathbf{k}}, \Psi^\dagger(\mathbf{r}')\} \{\Psi(\mathbf{r}), c_{n\mathbf{k}}^\dagger\} \\ &= \sum_{n=1}^{n_e} \sum_{\mathbf{k} \in BZ} \psi_{n\mathbf{k}}(\mathbf{r}) \psi_{n\mathbf{k}}^*(\mathbf{r}'). \end{aligned} \quad (\text{B4})$$

It's convenient to define the single-particle density operator

$$\hat{\rho} = \int d\mathbf{r} d\mathbf{r}' |\mathbf{r}\rangle \rho(\mathbf{r}, \mathbf{r}') \langle \mathbf{r}'| = \sum_{n=1}^{n_e} \sum_{\mathbf{k} \in BZ} |\psi_{n\mathbf{k}}\rangle \langle \psi_{n\mathbf{k}}| \quad (\text{B5})$$

and its k -dependent counterpart

$$\hat{\rho}_{\mathbf{k}} = \mathcal{N} e^{-i\mathbf{k} \cdot \hat{\mathbf{r}}} \hat{\rho} e^{i\mathbf{k} \cdot \hat{\mathbf{r}}} = \sum_{i=1}^{n_e} |u_{n\mathbf{k}}\rangle \langle u_{n\mathbf{k}}|. \quad (\text{B6})$$

Notice that the single particle Hilbert space \mathcal{H} of $\hat{\rho}$ is all kinds of functions while the Hilbert space $\mathcal{H}_{\mathbf{k}}$ of $\hat{\rho}_{\mathbf{k}}$ is only the cell-periodic functions. That's why the prefactor \mathcal{N} , number of cells, appears in the definition of $\hat{\rho}_{\mathbf{k}}$ in Eq. (B6). We will see the single-particle and interaction energies could be expressed as functionals of $\hat{\rho}_{\mathbf{k}}$ and therefore functionals of occupied states $|u_{n\mathbf{k}}\rangle$.

The single-particle part is

$$\begin{aligned} E_0 &\equiv \langle GS | H_0 | GS \rangle \\ &= \int d\mathbf{r} d\mathbf{r}' \delta(\mathbf{r} - \mathbf{r}') h^0(-i\nabla_{\mathbf{r}}, \mathbf{r}) \rho(\mathbf{r}, \mathbf{r}') \\ &= \sum_{n=1}^{n_e} \sum_{\mathbf{k} \in BZ} \int d\mathbf{r} \psi_{n\mathbf{k}}^*(\mathbf{r}) h^0(-i\nabla_{\mathbf{r}}, \mathbf{r}) \psi_{n\mathbf{k}}(\mathbf{r}) \\ &= \sum_{\mathbf{k} \in BZ} \text{Tr}[\hat{h}_{\mathbf{k}}^0 \hat{\rho}_{\mathbf{k}}], \end{aligned} \quad (\text{B7})$$

where $\hat{h}_{\mathbf{k}}^0 = e^{-i\mathbf{k} \cdot \hat{\mathbf{r}}} \hat{h}^0(\hat{\mathbf{p}}, \hat{\mathbf{r}}) e^{i\mathbf{k} \cdot \hat{\mathbf{r}}} = \hat{h}^0(\hat{\mathbf{p}} + \mathbf{k}, \hat{\mathbf{r}})$ is the k -dependent single particle Hamiltonian acting on cell-periodic functions with matrix elements

$$h_{mn\mathbf{k}}^0 \equiv \frac{1}{v_c} \int_{\text{cell}} d\mathbf{r} u_{m\mathbf{k}}^*(\mathbf{r}) h^0(-i\nabla_{\mathbf{r}} + \mathbf{k}, \mathbf{r}) u_{n\mathbf{k}}(\mathbf{r}). \quad (\text{B8})$$

Similarly, the interaction part is evaluated with the

help of Wick's theorem

$$\begin{aligned}
& \langle GS | H_I | GS \rangle \\
&= \frac{1}{2} \int d\mathbf{r} d\mathbf{r}' V(\mathbf{r} - \mathbf{r}') \langle \Psi^\dagger(\mathbf{r}) \Psi^\dagger(\mathbf{r}') \Psi(\mathbf{r}') \Psi(\mathbf{r}) \rangle \\
&= \frac{1}{2} \int d\mathbf{r} d\mathbf{r}' V(\mathbf{r} - \mathbf{r}') [\rho(\mathbf{r}, \mathbf{r}) \rho(\mathbf{r}', \mathbf{r}') - \rho(\mathbf{r}', \mathbf{r}) \rho(\mathbf{r}, \mathbf{r}')] \\
&= \frac{1}{2\mathcal{V}} \sum_{\mathbf{q}} V(\mathbf{q}) \int d\mathbf{r} d\mathbf{r}' e^{i\mathbf{q} \cdot (\mathbf{r} - \mathbf{r}')} \rho(\mathbf{r}, \mathbf{r}) \rho(\mathbf{r}', \mathbf{r}') \\
&\quad - \frac{1}{2\mathcal{V}} \sum_{\mathbf{q}} V(\mathbf{q}) \int d\mathbf{r} d\mathbf{r}' e^{i\mathbf{q} \cdot (\mathbf{r} - \mathbf{r}')} \rho(\mathbf{r}', \mathbf{r}) \rho(\mathbf{r}, \mathbf{r}'),
\end{aligned} \tag{B9}$$

where $V(\mathbf{q}) \equiv \int d\mathbf{r} V(\mathbf{r}) e^{-i\mathbf{q} \cdot \mathbf{r}}$ is the Fourier transformation of $V(\mathbf{r})$. The first part in Eq. (B9) is the Hartree energy and is simplified as

$$\begin{aligned}
E_H &= \frac{1}{2\mathcal{V}} \sum_{\mathbf{q}} V(\mathbf{q}) \int d\mathbf{r} d\mathbf{r}' e^{i\mathbf{q} \cdot (\mathbf{r} - \mathbf{r}')} \rho(\mathbf{r}, \mathbf{r}) \rho(\mathbf{r}', \mathbf{r}') \\
&= \frac{1}{2\mathcal{V}} \sum_{\mathbf{q}} V(\mathbf{q}) \int d\mathbf{r} e^{i\mathbf{q} \cdot \mathbf{r}} \sum_{n=1}^{n_e} \sum_{\mathbf{k}_1 \in BZ} \psi_{n\mathbf{k}_1}^*(\mathbf{r}) \psi_{n\mathbf{k}_1}(\mathbf{r}) \\
&\quad \times \int d\mathbf{r}' e^{-i\mathbf{q} \cdot \mathbf{r}'} \sum_{m=1}^{n_e} \sum_{\mathbf{k}_2 \in BZ} \psi_{m\mathbf{k}_2}^*(\mathbf{r}') \psi_{m\mathbf{k}_2}(\mathbf{r}') \\
&= \frac{1}{2\mathcal{V}} \sum_{\mathbf{k}_i \in BZ} \sum_{\mathbf{q}} V(\mathbf{q}) \delta_{\mathbf{q}\mathbf{G}} \text{Tr}[e^{i\mathbf{q} \cdot \hat{\mathbf{r}}} \hat{\rho}_{\mathbf{k}_1}] \text{Tr}[e^{-i\mathbf{q} \cdot \hat{\mathbf{r}}} \hat{\rho}_{\mathbf{k}_2}] \\
&= \frac{1}{2\mathcal{V}} \sum_{\mathbf{k}_i \in BZ, \mathbf{G}} V(\mathbf{G}) \text{Tr}[e^{i\mathbf{G} \cdot \hat{\mathbf{r}}} \hat{\rho}_{\mathbf{k}_1}] \text{Tr}[e^{-i\mathbf{G} \cdot \hat{\mathbf{r}}} \hat{\rho}_{\mathbf{k}_2}].
\end{aligned} \tag{B10}$$

where \mathbf{G} is reciprocal vector. The $e^{i\mathbf{G} \cdot \hat{\mathbf{r}}}$ term in Eq. (B10) should be understood as a single particle operator that acts on $|u_{n\mathbf{k}}\rangle$ as

$$\langle \mathbf{r} | e^{i\mathbf{G} \cdot \hat{\mathbf{r}}} | u_{n\mathbf{k}} \rangle = e^{i\mathbf{G} \cdot \mathbf{r}} u_{n\mathbf{k}}(\mathbf{r}) = u_{n\mathbf{k}-\mathbf{G}}(\mathbf{r}) = \langle \mathbf{r} | u_{n\mathbf{k}-\mathbf{G}} \rangle. \tag{B11}$$

The second part in Eq. (B9) is the Fock energy

$$\begin{aligned}
E_F &= -\frac{1}{2\mathcal{V}} \sum_{\mathbf{q}} V(\mathbf{q}) \int d\mathbf{r} d\mathbf{r}' e^{i\mathbf{q} \cdot (\mathbf{r} - \mathbf{r}')} \\
&\quad \times \sum_{m,n=1}^{n_e} \sum_{\mathbf{k}_i \in BZ} \psi_{n\mathbf{k}_1}(\mathbf{r}') \psi_{n\mathbf{k}_1}^*(\mathbf{r}) \psi_{m\mathbf{k}_2}(\mathbf{r}) \psi_{m\mathbf{k}_2}^*(\mathbf{r}') \\
&= \frac{-1}{2\mathcal{V}} \sum_{\mathbf{k}_i \in BZ, \mathbf{q}} V(\mathbf{q}) \delta_{\mathbf{q}\mathbf{k}_1 - \mathbf{k}_2 + \mathbf{G}} \text{Tr}[e^{-i\mathbf{G} \cdot \hat{\mathbf{r}}} \hat{\rho}_{\mathbf{k}_1} e^{i\mathbf{G} \cdot \hat{\mathbf{r}}} \hat{\rho}_{\mathbf{k}_2}] \\
&= \frac{-1}{2\mathcal{V}} \sum_{\mathbf{k}_i \in BZ, \mathbf{G}} V(\mathbf{k}_1 - \mathbf{k}_2 + \mathbf{G}) \text{Tr}[e^{-i\mathbf{G} \cdot \hat{\mathbf{r}}} \hat{\rho}_{\mathbf{k}_1} e^{i\mathbf{G} \cdot \hat{\mathbf{r}}} \hat{\rho}_{\mathbf{k}_2}].
\end{aligned} \tag{B12}$$

The polarization energy can't be expressed by density

operator $\hat{\rho}_{\mathbf{k}}$ but is still a functional of occupied states

$$\begin{aligned}
E_P &\equiv \langle GS | H_P | GS \rangle \\
&= e\mathcal{E} \cdot \int d\mathbf{r} \mathbf{r} \rho(\mathbf{r}, \mathbf{r}) \\
&= e\mathcal{E} \cdot \sum_{n=1}^{N_e} \sum_{\mathbf{k}, \mathbf{k}'} \delta_{\mathbf{k}, \mathbf{k}'} \int d\mathbf{r} \psi_{n\mathbf{k}'}^*(\mathbf{r}) \mathbf{r} \psi_{n\mathbf{k}}(\mathbf{r}) \\
&= e\mathcal{E} \cdot \sum_{n=1}^{N_e} \sum_{\mathbf{k}, \mathbf{k}'} \delta_{\mathbf{k}, \mathbf{k}'} \times \left[-i\nabla_{\mathbf{k}} \int d\mathbf{r} \psi_{n\mathbf{k}'}^*(\mathbf{r}) \psi_{n\mathbf{k}}(\mathbf{r}) \right. \\
&\quad \left. + \frac{1}{\mathcal{V}} \int d\mathbf{r} e^{i(\mathbf{k}-\mathbf{k}') \cdot \mathbf{r}} u_{n\mathbf{k}'}^*(\mathbf{r}) i\nabla_{\mathbf{k}} u_{n\mathbf{k}}(\mathbf{r}) \right] \\
&= e\mathcal{E} \cdot \sum_{n=1}^{N_e} \sum_{\mathbf{k}, \mathbf{k}'} \delta_{\mathbf{k}, \mathbf{k}'} [-i\nabla_{\mathbf{k}} \delta_{\mathbf{k}, \mathbf{k}'} + \langle u_{n\mathbf{k}} | i\nabla_{\mathbf{k}} u_{n\mathbf{k}} \rangle] \\
&= \sum_{n=1}^{n_e} \sum_{\mathbf{k}} \langle u_{n\mathbf{k}} | ie\mathcal{E} \cdot \nabla_{\mathbf{k}} | u_{n\mathbf{k}} \rangle.
\end{aligned} \tag{B13}$$

This result is consistent with the Berry phase definition of polarization. For a finite-size system with periodic boundary conditions, the polarization and the polarization energy should be written with the discrete form of Berry phase as [26]

$$E_P = \frac{-e\mathcal{E}}{\Delta k_{\parallel}} \text{Im} \sum_{\mathbf{k}} \log \det S(\mathbf{k}, \mathbf{k} + \Delta \mathbf{k}_{\parallel}), \tag{B14}$$

where $|\Delta \mathbf{k}_{\parallel}| = 2\pi/L$ and is along the direction of electric field. The overlap matrix S is defined as

$$S_{mn}(\mathbf{k}, \mathbf{k}') = \langle u_{m\mathbf{k}} | u_{n\mathbf{k}'} \rangle, \quad m, n = 1, 2, \dots, n_e. \tag{B15}$$

Appendix C: Mean Field Hamiltonian and Self-consistent Equation

The total energy as a functional of occupied bands $\{|u_{n\mathbf{k}}\rangle\}_{n=1}^{n_e}$ is written as

$$E_{tot}[|u_{n\mathbf{k}}\rangle; \mathcal{E}] = E_0[\hat{\rho}_{\mathbf{k}}] + E_{HF}[\hat{\rho}_{\mathbf{k}}] + E_P[|u_{n\mathbf{k}}\rangle; \mathcal{E}] \tag{C1}$$

and the stationary state is found by minimize E_{tot} with constraints

$$\langle u_{m\mathbf{k}} | u_{n\mathbf{k}} \rangle = \delta_{mn}. \tag{C2}$$

By introduce Lagrange multipliers $\xi_{n\mathbf{k}}$, the constrained minimization of E_{tot} is transformed into an unconstrained minimization of

$$F[|u_{n\mathbf{k}}\rangle; \mathcal{E}] \equiv E_{tot}[|u_{n\mathbf{k}}\rangle; \mathcal{E}] + \sum_{n\mathbf{k}} \xi_{n\mathbf{k}} (1 - \langle u_{n\mathbf{k}} | u_{n\mathbf{k}} \rangle). \tag{C3}$$

Let's calculate the unconstrained derivatives of F with respect to $\langle u_{n\mathbf{k}} |$. We first show that

$$\begin{aligned}
\frac{\delta \text{Tr}[\hat{\rho}_{\mathbf{k}_2} \hat{\rho}_{\mathbf{k}_2}]}{\delta \langle u_{n\mathbf{k}_1} |} &= \frac{\delta}{\delta \langle u_{n\mathbf{k}_1} |} \sum_m \langle u_{n\mathbf{k}_2} | \hat{\rho}_{\mathbf{k}_2} | u_{n\mathbf{k}_2} \rangle \\
&= \delta_{\mathbf{k}_1 \mathbf{k}_2} \hat{\rho}_{\mathbf{k}_2} | u_{n\mathbf{k}_2} \rangle.
\end{aligned} \tag{C4}$$

The single-particle, Hartree, and Fock energy functionals all take this form thus are easily evaluated

$$\frac{\delta E_0}{\delta \langle u_{n\mathbf{k}} |} = \hat{h}_{\mathbf{k}}^0 |u_{n\mathbf{k}}\rangle, \quad (\text{C5})$$

$$\frac{\delta E_H}{\delta \langle u_{n\mathbf{k}} |} = \frac{1}{\mathcal{V}} \sum_{\mathbf{k}_2 \in BZ, G} V(\mathbf{G}) \text{Tr}[\hat{\rho}_{\mathbf{k}_2} e^{-i\mathbf{G} \cdot \hat{\mathbf{r}}} e^{i\mathbf{G} \cdot \hat{\mathbf{r}}} |u_{n\mathbf{k}}\rangle, \quad (\text{C6})$$

$$\frac{\delta E_F}{\delta \langle u_{n\mathbf{k}} |} = -\frac{1}{\mathcal{V}} \sum_{\mathbf{k}_2 \in BZ, G} V(\mathbf{k} - \mathbf{k}_2 + \mathbf{G}) \times e^{i\mathbf{G} \cdot \hat{\mathbf{r}}} \hat{\rho}_{\mathbf{k}_2} e^{-i\mathbf{G} \cdot \hat{\mathbf{r}}} |u_{n\mathbf{k}}\rangle. \quad (\text{C7})$$

From the expression above, we could define the Hartree and Fock Hamiltonian as

$$\hat{h}_{\mathbf{k}}^H[\hat{\rho}_{\mathbf{k}}] = \frac{1}{\mathcal{V}} \sum_{\mathbf{k}_2 \in BZ, G} V(\mathbf{G}) \text{Tr}[\hat{\rho}_{\mathbf{k}_2} e^{-i\mathbf{G} \cdot \hat{\mathbf{r}}} e^{i\mathbf{G} \cdot \hat{\mathbf{r}}}, \quad (\text{C8})$$

$$\hat{h}_{\mathbf{k}}^F[\hat{\rho}_{\mathbf{k}}] = -\frac{1}{\mathcal{V}} \sum_{\mathbf{k}_2 \in BZ, G} V(\mathbf{k} - \mathbf{k}_2 + \mathbf{G}) e^{i\mathbf{G} \cdot \hat{\mathbf{r}}} \hat{\rho}_{\mathbf{k}_2} e^{-i\mathbf{G} \cdot \hat{\mathbf{r}}}. \quad (\text{C9})$$

As functionals of gauge invariant single-particle density operator $\hat{\rho}_{\mathbf{k}}$, the Hartree and Fock Hamiltonian defined in Eq. (C8)(C9) are also invariant under k -space gauge transform of the occupied bands.

As for the polarization term, we start from the discrete form Eq. (B14) and take the thermodynamic limit later. The unconstrained derivatives of E_P is

$$\begin{aligned} \frac{\delta E_P}{\delta \langle u_{n\mathbf{k}} |} &= \frac{-e\mathcal{E}}{2i\Delta k_{\parallel}} \frac{\delta}{\delta \langle u_{n\mathbf{k}} |} \left[\sum_{\sigma=\pm} \sigma \sum_{\mathbf{k}} \log \det S(\mathbf{k}, \mathbf{k}_{\sigma}) \right] \\ &= \frac{ie\mathcal{E}}{2\Delta k_{\parallel}} \frac{\delta}{\delta \langle u_{n\mathbf{k}} |} \left[\sum_{\sigma=\pm} \sigma \sum_{\mathbf{k}} \text{Tr} \log S(\mathbf{k}, \mathbf{k}_{\sigma}) \right] \\ &= \frac{ie\mathcal{E}}{2\Delta k_{\parallel}} \sum_{\sigma=\pm} \sigma \text{Tr} \left[\frac{\delta S(\mathbf{k}, \mathbf{k}_{\sigma})}{\delta \langle u_{n\mathbf{k}} |} S^{-1}(\mathbf{k}, \mathbf{k}_{\sigma}) \right] \\ &= \frac{ie\mathcal{E}}{2\Delta k_{\parallel}} \sum_{\sigma=\pm} \sigma \sum_{m=1}^{n_e} |u_{m\mathbf{k}_{\sigma}}\rangle S_{mn}^{-1}(\mathbf{k}, \mathbf{k}_{\sigma}), \end{aligned} \quad (\text{C10})$$

where abbreviation $\mathbf{k}_{\sigma} = \mathbf{k} + \sigma\Delta\mathbf{k}_{\parallel}$ is used for simplicity. Denote $|D_{n\mathbf{k}}\rangle = \delta E_P / \delta \langle u_{n\mathbf{k}} |$. Easy to see that

$$\begin{aligned} \langle u_{l\mathbf{k}} | D_{n\mathbf{k}} \rangle &= \frac{ie\mathcal{E}}{2\Delta k_{\parallel}} \sum_{\sigma} \sigma \sum_{m=1}^{n_e} S_{lm}(\mathbf{k}, \mathbf{k}_{\sigma}) S_{mn}^{-1}(\mathbf{k}, \mathbf{k}_{\sigma}) \\ &= \frac{ie\mathcal{E}}{2\Delta k_{\parallel}} \sum_{\sigma} \sigma \delta_{ln} \\ &= 0. \end{aligned} \quad (\text{C11})$$

So polarization Hamiltonian could be defined as

$$\hat{h}_{\mathbf{k}}^P[|u_{n\mathbf{k}}\rangle; \mathcal{E}] = \sum_{n=1}^{n_e} |D_{n\mathbf{k}}\rangle \langle u_{n\mathbf{k}}| + h.c. \quad (\text{C12})$$

and satisfies

$$\hat{h}_{\mathbf{k}}^P |u_{n\mathbf{k}}\rangle = \sum_{m=1}^{n_e} |D_{m\mathbf{k}}\rangle \delta_{mn} = |D_{n\mathbf{k}}\rangle = \frac{\delta E_P}{\delta \langle u_{n\mathbf{k}} |}. \quad (\text{C13})$$

Before processing, one should verify that this definition of polarization Hamiltonian is a gauge invariant. By denoting $\Phi_{\mathbf{k}}^{\dagger} = [|u_{1\mathbf{k}}\rangle, \dots, |u_{n_e\mathbf{k}}\rangle]$, the polarization Hamiltonian is written in a more neat form

$$\hat{h}_{\mathbf{k}}^P = \frac{ie\mathcal{E}}{2\Delta k_{\parallel}} \sum_{\sigma=\pm} \sigma \Phi_{\mathbf{k}_{\sigma}} (\Phi_{\mathbf{k}}^{\dagger} \Phi_{\mathbf{k}_{\sigma}})^{-1} \Phi_{\mathbf{k}}^{\dagger} + h.c.. \quad (\text{C14})$$

A k -space gauge transformation $(U_{\mathbf{k}})_{n_e \times n_e}$ on occupied bands will transform $\Phi_{\mathbf{k}}$ into $\Phi_{\mathbf{k}} U_{\mathbf{k}}$ and the polarization Hamiltonian becomes

$$\begin{aligned} (\hat{h}_{\mathbf{k}}^P)' &= \frac{ie\mathcal{E}}{2\Delta k_{\parallel}} \sum_{\sigma=\pm} \sigma \Phi_{\mathbf{k}_{\sigma}} U_{\mathbf{k}_{\sigma}} (U_{\mathbf{k}}^{\dagger} \Phi_{\mathbf{k}}^{\dagger} \Phi_{\mathbf{k}_{\sigma}} U_{\mathbf{k}_{\sigma}})^{-1} U_{\mathbf{k}}^{\dagger} \Phi_{\mathbf{k}}^{\dagger} + h.c. \\ &= \frac{ie\mathcal{E}}{2\Delta k_{\parallel}} \sum_{\sigma=\pm} \sigma \Phi_{\mathbf{k}_{\sigma}} U_{\mathbf{k}_{\sigma}} U_{\mathbf{k}_{\sigma}}^{-1} (\Phi_{\mathbf{k}}^{\dagger} \Phi_{\mathbf{k}_{\sigma}})^{-1} (U_{\mathbf{k}}^{\dagger})^{-1} U_{\mathbf{k}}^{\dagger} \Phi_{\mathbf{k}}^{\dagger} + h.c. \\ &= \hat{h}_{\mathbf{k}}^P, \end{aligned} \quad (\text{C15})$$

which is invariant.

It's easier to see this gauge invariance in the thermodynamic limit $L \rightarrow \infty$ and $\Delta k_{\parallel} \rightarrow 0$. At this limit

$$S_{mn}(\mathbf{k}, \mathbf{k}_{\sigma}) = \delta_{mn} + \sigma \langle u_{m\mathbf{k}} | \partial_{k_{\parallel}} u_{n\mathbf{k}} \rangle dk, \quad (\text{C16a})$$

$$S_{mn}^{-1}(\mathbf{k}, \mathbf{k}_{\sigma}) = \delta_{mn} - \sigma \langle u_{m\mathbf{k}} | \partial_{k_{\parallel}} u_{n\mathbf{k}} \rangle dk. \quad (\text{C16b})$$

So

$$\begin{aligned} |D_{n\mathbf{k}}\rangle &= \frac{ie\mathcal{E}}{2\Delta k_{\parallel}} \sum_{\sigma=\pm} \sigma \sum_{m=1}^{n_e} (|u_{m\mathbf{k}}\rangle + \sigma |\partial_{k_{\parallel}} u_{m\mathbf{k}}\rangle dk) \\ &\quad \times (\delta_{mn} - \sigma \langle u_{m\mathbf{k}} | \partial_{k_{\parallel}} u_{n\mathbf{k}} \rangle dk) \\ &= ie\mathcal{E} \sum_{m=1}^{n_e} [|\partial_{k_{\parallel}} u_{m\mathbf{k}}\rangle \delta_{mn} - |u_{m\mathbf{k}}\rangle \langle u_{m\mathbf{k}} | \partial_{k_{\parallel}} u_{n\mathbf{k}} \rangle] \\ &= ie\mathcal{E} (1 - \hat{\rho}_{\mathbf{k}}) |\partial_{k_{\parallel}} u_{n\mathbf{k}}\rangle \end{aligned} \quad (\text{C17})$$

and the polarization Hamiltonian in thermodynamic limit is written as

$$\begin{aligned} \lim_{\Delta k \rightarrow 0} \hat{h}_{\mathbf{k}}^P &= ie\mathcal{E} \sum_n^{N_e} (1 - \hat{\rho}_{\mathbf{k}}) |\partial_{k_{\parallel}} u_{n\mathbf{k}}\rangle \langle u_{n\mathbf{k}}| + h.c. \\ &= ie\mathcal{E} (1 - \hat{\rho}_{\mathbf{k}}) \partial_{k_{\parallel}} \hat{\rho}_{\mathbf{k}} + h.c. \\ &= ie\mathcal{E} \cdot [\nabla_{\mathbf{k}} \hat{\rho}_{\mathbf{k}}]. \end{aligned} \quad (\text{C18})$$

The thermodynamic limit expression Eq. (C18) is only a functional of the gauge invariant $\hat{\rho}_{\mathbf{k}}$ and thus is also a gauge invariant.

Finally, minimization of $F[|u_{n\mathbf{k}}\rangle; \mathcal{E}]$ gives us the self-consistent equation

$$\frac{\delta F}{\delta \langle u_{n\mathbf{k}} |} = 0 \implies \hat{h}_{\mathbf{k}}^{MF}[|u_{n\mathbf{k}}\rangle; \mathcal{E}] |u_{n\mathbf{k}}\rangle = \xi_{n\mathbf{k}} |u_{n\mathbf{k}}\rangle \quad (\text{C19})$$

where the mean field Hamiltonian is

$$\hat{h}_{\mathbf{k}}^{MF} = \hat{h}_{\mathbf{k}}^0 + \hat{h}_{\mathbf{k}}^H[\hat{\rho}_{\mathbf{k}}] + \hat{h}_{\mathbf{k}}^F[\hat{\rho}_{\mathbf{k}}] + \hat{h}_{\mathbf{k}}^P[|u_{n\mathbf{k}}\rangle; \mathcal{E}]. \quad (\text{C20})$$

Appendix D: The Hessian Matrix

Assume $\mathcal{E} < \mathcal{E}_c$, and the self consistent equation has solutions

$$h_{\mathbf{k}}^{MF}[|v\mathbf{k}; \mathcal{E}\rangle][i\mathbf{k}; \mathcal{E}] = \xi_{i\mathbf{k}; \mathcal{E}}[i\mathbf{k}; \mathcal{E}], \quad i = c, v. \quad (\text{D1})$$

The valence band $|v\mathbf{k}; \mathcal{E}\rangle$ is chosen as the one with lower band energy, i.e. $\xi_{v\mathbf{k}; \mathcal{E}} < \xi_{c\mathbf{k}; \mathcal{E}}$. The \mathcal{E} label in wavefunctions and band energies means they are converged solutions.

At the converged point (local minimum of the total energy functional), the trial HF state could be reparametrized as

$$|v'\mathbf{k}; \mathcal{E}\rangle = \frac{|v\mathbf{k}; \mathcal{E}\rangle + f_{\mathbf{k}}|c\mathbf{k}; \mathcal{E}\rangle}{\sqrt{1 + |f_{\mathbf{k}}|^2}}, \quad (\text{D2})$$

where $f_{\mathbf{k}}$ is arbitrary complex-valued function defined on Brillouin zone. This parametrization is unconstrained and complete, and the total energy then becomes functional of $f_{\mathbf{k}}$ as

$$\varepsilon_{tot}[f_{\mathbf{k}}^*, f_{\mathbf{k}}; \mathcal{E}] \equiv \varepsilon_{tot}[|v'\mathbf{k}; \mathcal{E}\rangle; \mathcal{E}]. \quad (\text{D3})$$

By writing $f_{\mathbf{k}} = f_{\mathbf{k},r} + if_{\mathbf{k},i}$, where $f_{\mathbf{k},r}$ and $f_{\mathbf{k},i}$ are real variables, the Hessian matrix is defined as

$$\mathbf{H}_{\mathbf{k}\mathbf{k}'} = \begin{pmatrix} \frac{\delta^2 \varepsilon_{tot}}{\delta f_{\mathbf{k},r} \delta f_{\mathbf{k}',r}} & \frac{\delta^2 \varepsilon_{tot}}{\delta f_{\mathbf{k},r} \delta f_{\mathbf{k}',i}} \\ \frac{\delta^2 \varepsilon_{tot}}{\delta f_{\mathbf{k},i} \delta f_{\mathbf{k}',r}} & \frac{\delta^2 \varepsilon_{tot}}{\delta f_{\mathbf{k},i} \delta f_{\mathbf{k}',i}} \end{pmatrix}. \quad (\text{D4})$$

For simplicity, the \mathcal{E} label will be omitted in the following derivations.

We first calculate the derivatives of $|v'\mathbf{k}\rangle$ with respect to $f_{\mathbf{k},r/i}$ for further usage.

$$\frac{\delta |v'\mathbf{k}\rangle}{\delta f_{\mathbf{k},r}} = \frac{-f_{\mathbf{k},r}|v\mathbf{k}\rangle + (1 - if_{\mathbf{k},i}f_{\mathbf{k}})|c\mathbf{k}\rangle}{(1 + |f_{\mathbf{k}}|^2)^{3/2}}, \quad (\text{D5})$$

$$\frac{\delta |v'\mathbf{k}\rangle}{\delta f_{\mathbf{k},i}} = \frac{-f_{\mathbf{k},i}|v\mathbf{k}\rangle + i(1 + f_{\mathbf{k},r}f_{\mathbf{k}})|c\mathbf{k}\rangle}{(1 + |f_{\mathbf{k}}|^2)^{3/2}}. \quad (\text{D6})$$

At $f_{\mathbf{k}} = 0$, they are simplified as

$$\left. \frac{\delta |v'\mathbf{k}\rangle}{\delta f_{\mathbf{k},r}} \right|_{f_{\mathbf{k}}=0} = |c\mathbf{k}\rangle, \quad (\text{D7})$$

$$\left. \frac{\delta |v'\mathbf{k}\rangle}{\delta f_{\mathbf{k},i}} \right|_{f_{\mathbf{k}}=0} = i|c\mathbf{k}\rangle. \quad (\text{D8})$$

The second order derivatives of $|v'\mathbf{k}\rangle$ at $f_{\mathbf{k}} = 0$ are

$$\left. \frac{\delta^2 |v'\mathbf{k}\rangle}{\delta f_{\mathbf{k},r} \delta f_{\mathbf{k}',r}} \right|_{f_{\mathbf{k}}=0} = -\delta_{\mathbf{k}\mathbf{k}'}|v\mathbf{k}\rangle, \quad (\text{D9})$$

$$= \left. \frac{\delta^2 |v'\mathbf{k}\rangle}{\delta f_{\mathbf{k},i} \delta f_{\mathbf{k}',i}} \right|_{f_{\mathbf{k}}=0} = -\delta_{\mathbf{k}\mathbf{k}'}|v\mathbf{k}\rangle, \quad (\text{D10})$$

$$\left. \frac{\delta^2 |v'\mathbf{k}\rangle}{\delta f_{\mathbf{k},r} \delta f_{\mathbf{k}',i}} \right|_{f_{\mathbf{k}}=0} = 0. \quad (\text{D11})$$

The first order derivative of ε_{tot} defined by Eq. (5) is

$$\begin{aligned} \frac{\delta \varepsilon_{tot}}{\delta f_{\mathbf{k},r/i}} &= \frac{\delta \langle v'\mathbf{k} |}{\delta f_{\mathbf{k},r/i}} \frac{\delta \varepsilon_{tot}}{\delta \langle v'\mathbf{k} |} + c.c. \\ &= \frac{1}{\mathcal{V}} \frac{\delta \langle v'\mathbf{k} |}{\delta f_{\mathbf{k},r/i}} h_{\mathbf{k}}^{MF}[|v'\mathbf{k}\rangle][v'\mathbf{k}] + c.c.. \end{aligned} \quad (\text{D12})$$

We use the definition of mean field Hamiltonian $h_{\mathbf{k}}^{MF}[|v\mathbf{k}\rangle][v\mathbf{k}] \equiv \mathcal{V} \delta \varepsilon_{tot} / \delta \langle v\mathbf{k} |$ for the last equality in Eq. (D12). At $f_{\mathbf{k}} = 0$, the first-order derivative is just

$$\left. \frac{\delta \varepsilon_{tot}}{\delta f_{\mathbf{k},r/i}} \right|_{f_{\mathbf{k}}=0} \propto \langle c\mathbf{k} | h_{\mathbf{k}}^{MF}[|v\mathbf{k}\rangle][v\mathbf{k}] + c.c. = 0,$$

which is consistent with the fact that $|v\mathbf{k}\rangle$ is a local minimum.

Then let's evaluate second-order derivatives of ε_{tot}

$$\begin{aligned} &\mathcal{V} \left. \frac{\delta^2 \varepsilon_{tot}}{\delta f_{\mathbf{k},r} \delta f_{\mathbf{k}',r}} \right|_{f_{\mathbf{k}}=0} \\ &= \left. \frac{\delta \langle v'\mathbf{k} |}{\delta f_{\mathbf{k},r}} \right|_{f_{\mathbf{k}}=0} \left. \frac{\delta h_{\mathbf{k}}^{MF}[|v'\mathbf{k}\rangle]}{\delta f_{\mathbf{k}',r}} \right|_{f_{\mathbf{k}}=0} |v'\mathbf{k}\rangle \\ &\quad + \left. \frac{\delta \langle v'\mathbf{k} |}{\delta f_{\mathbf{k},r}} \right|_{f_{\mathbf{k}}=0} h_{\mathbf{k}}^{MF}[|v'\mathbf{k}\rangle] \left. \frac{\delta |v'\mathbf{k}\rangle}{\delta f_{\mathbf{k}',r}} \right|_{f_{\mathbf{k}}=0} \\ &\quad + \left. \frac{\delta^2 \langle v'\mathbf{k} |}{\delta f_{\mathbf{k},r} \delta f_{\mathbf{k}',r}} \right|_{f_{\mathbf{k}}=0} h_{\mathbf{k}}^{MF}[|v'\mathbf{k}\rangle][v'\mathbf{k}] + c.c. \\ &= \delta_{\mathbf{k}\mathbf{k}'}(\xi_{c\mathbf{k}} - \xi_{v\mathbf{k}}) + \langle c\mathbf{k} | \left. \frac{\delta h_{\mathbf{k}}^{MF}[|v'\mathbf{k}\rangle]}{\delta f_{\mathbf{k}',r}} \right|_{f_{\mathbf{k}}=0} |v\mathbf{k}\rangle + c.c.. \end{aligned}$$

Similarly,

$$\begin{aligned} &\mathcal{V} \left. \frac{\delta^2 \varepsilon_{tot}}{\delta f_{\mathbf{k},i} \delta f_{\mathbf{k}',i}} \right|_{f_{\mathbf{k}}=0} \\ &= \delta_{\mathbf{k}\mathbf{k}'}(\xi_{c\mathbf{k}} - \xi_{v\mathbf{k}}) - i \langle c\mathbf{k} | \left. \frac{\delta h_{\mathbf{k}}^{MF}[|v'\mathbf{k}\rangle]}{\delta f_{\mathbf{k}',i}} \right|_{f_{\mathbf{k}}=0} |v\mathbf{k}\rangle + c.c. \end{aligned}$$

and

$$\mathcal{V} \left. \frac{\delta^2 \varepsilon_{tot}}{\delta f_{\mathbf{k},r} \delta f_{\mathbf{k}',i}} \right|_{f_{\mathbf{k}}=0} = \langle c\mathbf{k} | \left. \frac{\delta h_{\mathbf{k}}^{MF}[|v'\mathbf{k}\rangle]}{\delta f_{\mathbf{k}',i}} \right|_{f_{\mathbf{k}}=0} |v\mathbf{k}\rangle + c.c..$$

So the final task is to evaluate the derivatives of $h_{\mathbf{k}}^{MF}$ with respect to $f_{\mathbf{k},r/i}$.

The Hartree one is

$$\begin{aligned} &\langle c\mathbf{k} | \left. \frac{\delta h_{\mathbf{k}}^H}{\delta f_{\mathbf{k}',r}} \right|_{f_{\mathbf{k}}=0} |v\mathbf{k}\rangle \\ &= \frac{4\pi e^2 d \langle c\mathbf{k} | e \rangle \langle e | v\mathbf{k} \rangle}{\epsilon} \left. \frac{\delta n_{ex}}{\delta f_{\mathbf{k}',r}} \right|_{f_{\mathbf{k}}=0} \\ &= \frac{4\pi e^2 d \langle c\mathbf{k} | e \rangle \langle e | v\mathbf{k} \rangle}{\epsilon} \left[\left. \frac{\delta \langle v'\mathbf{k} |}{\delta f_{\mathbf{k}',r}} \frac{\delta n_{ex}}{\delta \langle v'\mathbf{k} |}} \right|_{f_{\mathbf{k}}=0} + c.c. \right] \\ &= \frac{4\pi e^2 d \langle c\mathbf{k} | e \rangle \langle e | v\mathbf{k} \rangle}{\epsilon} \left[\frac{1}{\mathcal{V}} \langle c\mathbf{k}' | e \rangle \langle e | v\mathbf{k}' \rangle + c.c. \right] \\ &= \frac{2}{\mathcal{V}} \frac{4\pi e^2 d \langle c\mathbf{k} | e \rangle \langle e | v\mathbf{k} \rangle}{\epsilon} \text{Re}[\langle c\mathbf{k}' | e \rangle \langle e | v\mathbf{k}' \rangle] \end{aligned}$$

and

$$\begin{aligned} & \langle c\mathbf{k} | \frac{\delta h^H}{\delta f_{\mathbf{k}',i}} \Big|_{f_{\mathbf{k}}=0} | v\mathbf{k} \rangle \\ &= \frac{4\pi e^2 d \langle c\mathbf{k} | e \rangle \langle e | v\mathbf{k} \rangle}{\epsilon} \left[-i \frac{1}{V} \langle c\mathbf{k}' | e \rangle \langle e | v\mathbf{k}' \rangle + c.c. \right] \\ &= \frac{2}{V} \frac{4\pi e^2 d \langle c\mathbf{k} | e \rangle \langle e | v\mathbf{k} \rangle}{\epsilon} \text{Im}[\langle c\mathbf{k}' | e \rangle \langle e | v\mathbf{k}' \rangle]. \end{aligned}$$

The Fock one is

$$\begin{aligned} & \langle c\mathbf{k} | \frac{\delta h_{\mathbf{k}}^F}{\delta f_{\mathbf{k}',r}} \Big|_{f_{\mathbf{k}}=0} | v\mathbf{k} \rangle \\ &= -\frac{1}{V} \sum_{ss'} V_{s's}(\mathbf{k} - \mathbf{k}') \langle c\mathbf{k} | s \rangle \langle s' | v\mathbf{k} \rangle \frac{\delta \rho_{ss'\mathbf{k}'}}{\delta f_{\mathbf{k}',r}} \Big|_{f_{\mathbf{k}}=0} \\ &= -\frac{1}{V} \sum_{ss'} V_{s's}(\mathbf{k} - \mathbf{k}') \langle c\mathbf{k} | s \rangle \langle s' | v\mathbf{k} \rangle \\ & \quad \times (\langle v\mathbf{k}' | s' \rangle \langle s | c\mathbf{k}' \rangle + \langle c\mathbf{k}' | s' \rangle \langle s | v\mathbf{k}' \rangle) \end{aligned}$$

and

$$\begin{aligned} & \langle c\mathbf{k} | \frac{\delta h_{ss'\mathbf{k}}^F}{\delta f_{\mathbf{k}',i}} \Big|_{f_{\mathbf{k}}=0} | v\mathbf{k} \rangle \\ &= -\frac{i}{V} \sum_{ss'} V_{s's}(\mathbf{k} - \mathbf{k}') \langle c\mathbf{k} | s \rangle \langle s' | v\mathbf{k} \rangle \\ & \quad \times (\langle v\mathbf{k}' | s' \rangle \langle s | c\mathbf{k}' \rangle - \langle c\mathbf{k}' | s' \rangle \langle s | v\mathbf{k}' \rangle). \end{aligned}$$

As for the polarization term, use the fact that

$$\langle c\mathbf{k} | h_{\mathbf{k}}^P \frac{\delta | v\mathbf{k} \rangle}{\delta f_{\mathbf{k}'}} \Big|_{f_{\mathbf{k}}=0} \propto \delta_{\mathbf{k}\mathbf{k}'} \langle c\mathbf{k} | h_{\mathbf{k}}^P | c\mathbf{k} \rangle = 0,$$

we have

$$\begin{aligned} & \langle c\mathbf{k} | \frac{\delta h_{\mathbf{k}}^P}{\delta f_{\mathbf{k}',r}} \Big|_{f_{\mathbf{k}}=0} | v\mathbf{k} \rangle = \langle c\mathbf{k} | \frac{\delta (h_{\mathbf{k}}^P | v\mathbf{k} \rangle)}{\delta f_{\mathbf{k}',r}} \Big|_{f_{\mathbf{k}}=0} \\ &= \langle c\mathbf{k} | \frac{\delta}{\delta f_{\mathbf{k}',r}} \left[\frac{ie\mathcal{E}}{2\Delta k_{\parallel}} \sum_{\sigma=\pm 1} \frac{\sigma | v\mathbf{k}_{\sigma} \rangle}{\langle v\mathbf{k} | v\mathbf{k}_{\sigma} \rangle} \right] \Big|_{f_{\mathbf{k}}=0} \\ &= \frac{ie\mathcal{E}}{2\Delta k_{\parallel}} \sum_{\sigma=\pm} \sigma \left[\delta_{\mathbf{k}'\mathbf{k}_{\sigma}} \frac{\langle c\mathbf{k} | c\mathbf{k}_{\sigma} \rangle}{\langle v\mathbf{k} | v\mathbf{k}_{\sigma} \rangle} - \delta_{\mathbf{k}'\mathbf{k}} \frac{(\langle c\mathbf{k} | v\mathbf{k}_{\sigma} \rangle)^2}{(\langle v\mathbf{k} | v\mathbf{k}_{\sigma} \rangle)^2} \right. \\ & \quad \left. - \delta_{\mathbf{k}'\mathbf{k}_{\sigma}} \frac{\langle c\mathbf{k} | v\mathbf{k}_{\sigma} \rangle \langle v\mathbf{k} | c\mathbf{k}_{\sigma} \rangle}{(\langle v\mathbf{k} | v\mathbf{k}_{\sigma} \rangle)^2} \right] \end{aligned}$$

and

$$\begin{aligned} & \langle c\mathbf{k} | \frac{\delta h_{\mathbf{k}}^P}{\delta f_{\mathbf{k}',i}} \Big|_{f_{\mathbf{k}}=0} | v\mathbf{k} \rangle \\ &= \frac{ie\mathcal{E}}{2\Delta k_{\parallel}} \sum_{\sigma=\pm} \sigma \left[i\delta_{\mathbf{k}'\mathbf{k}_{\sigma}} \frac{\langle c\mathbf{k} | c\mathbf{k}_{\sigma} \rangle}{\langle v\mathbf{k} | v\mathbf{k}_{\sigma} \rangle} + i\delta_{\mathbf{k}'\mathbf{k}} \frac{(\langle c\mathbf{k} | v\mathbf{k}_{\sigma} \rangle)^2}{(\langle v\mathbf{k} | v\mathbf{k}_{\sigma} \rangle)^2} \right. \\ & \quad \left. - i\delta_{\mathbf{k}'\mathbf{k}_{\sigma}} \frac{\langle c\mathbf{k} | v\mathbf{k}_{\sigma} \rangle \langle v\mathbf{k} | c\mathbf{k}_{\sigma} \rangle}{(\langle v\mathbf{k} | v\mathbf{k}_{\sigma} \rangle)^2} \right]. \end{aligned}$$

Appendix E: Goldstone Mode

The many-body Hamiltonian Eq. (3) is invariant under gauge transformations of the electron creation operators: $c_{e\mathbf{k}}^{\dagger} \rightarrow e^{i\phi_e} c_{e\mathbf{k}}^{\dagger}$, $c_{h\mathbf{k}}^{\dagger} \rightarrow e^{i\phi_h} c_{h\mathbf{k}}^{\dagger}$. This $U(1) \times U(1)$ symmetry corresponds to the charge conservation in each layer.

After this gauge transformation, the valance band electron creation operator becomes

$$(c_{v\mathbf{k}}^{\dagger})' = \alpha_{\mathbf{k}} e^{i\phi_e} c_{e\mathbf{k}}^{\dagger} + \beta_{\mathbf{k}} e^{i\phi_h} c_{h\mathbf{k}}^{\dagger}, \quad (\text{E1})$$

which gives a new trial wavefunction

$$|v'\mathbf{k}\rangle = \begin{bmatrix} e^{i\phi_e} \alpha_{\mathbf{k}} \\ e^{i\phi_h} \beta_{\mathbf{k}} \end{bmatrix} = e^{i\phi} \begin{bmatrix} e^{i\phi_{ex}} \alpha_{\mathbf{k}} \\ e^{-i\phi_{ex}} \beta_{\mathbf{k}} \end{bmatrix}, \quad (\text{E2})$$

where $\phi = (\phi_e + \phi_h)/2$, $\phi_{ex} = (\phi_e - \phi_h)/2$ are related to the conservation of total charge and exciton number respectively. The relative density matrix $\tilde{\rho} = \rho - \rho^0$ transforms into

$$\tilde{\rho}'_{\mathbf{k}} = \begin{bmatrix} |\alpha_{\mathbf{k}}|^2 & e^{i(\phi_e - \phi_h)} \alpha_{\mathbf{k}} \beta_{\mathbf{k}}^* \\ e^{i(\phi_h - \phi_e)} \alpha_{\mathbf{k}}^* \beta_{\mathbf{k}} & |\beta_{\mathbf{k}}|^2 - 1 \end{bmatrix}, \quad (\text{E3})$$

or equivalently, $\tilde{\rho}'_{ss'\mathbf{k}} = e^{i(\phi_s - \phi_{s'})} \tilde{\rho}_{ss'\mathbf{k}}$. Besides, the overlap matrix $S(\mathbf{k}, \mathbf{k}') = \langle v\mathbf{k} | v\mathbf{k}' \rangle$ becomes

$$S'(\mathbf{k}, \mathbf{k}') = \langle v'\mathbf{k} | v'\mathbf{k}' \rangle = \alpha_{\mathbf{k}}^* \alpha_{\mathbf{k}'} + \beta_{\mathbf{k}}^* \beta_{\mathbf{k}'} = S(\mathbf{k}, \mathbf{k}'). \quad (\text{E4})$$

Substitute Eq. (E3)(E4) into the total energy expression Eq. (5) we find that

$$\begin{aligned} & \varepsilon_{tot}[|v'\mathbf{k}\rangle; \mathcal{E}] \\ &= \frac{1}{V} \sum_{s\mathbf{k}} h_{ss\mathbf{k}}^0 \tilde{\rho}'_{ss\mathbf{k}} + \frac{-e\mathcal{E}}{V\Delta k_{\parallel}} \text{Im} \sum_{\mathbf{k}_{\perp}} \log \prod_{\mathbf{k}_{\parallel}} \langle v'\mathbf{k} | v'\mathbf{k} + \Delta\mathbf{k}_{\parallel} \rangle \\ & \quad + \frac{2\pi e^2 n_{ex}^2 d}{\epsilon} - \frac{1}{2V^2} \sum_{ss'\mathbf{k}_1\mathbf{k}_2} V_{ss'}(\mathbf{k}_1 - \mathbf{k}_2) \tilde{\rho}'_{ss'\mathbf{k}_1} \tilde{\rho}'_{s'\mathbf{k}_2} \\ &= \frac{1}{V} \sum_{s\mathbf{k}} h_{ss\mathbf{k}}^0 \tilde{\rho}_{ss\mathbf{k}} + \frac{-e\mathcal{E}}{V\Delta k_{\parallel}} \text{Im} \sum_{\mathbf{k}_{\perp}} \log \prod_{\mathbf{k}_{\parallel}} \langle v\mathbf{k} | v\mathbf{k} + \Delta\mathbf{k}_{\parallel} \rangle \\ & \quad + \frac{2\pi e^2 n_{ex}^2 d}{\epsilon} - \frac{1}{2V^2} \sum_{ss'\mathbf{k}_1\mathbf{k}_2} V_{ss'}(\mathbf{k}_1 - \mathbf{k}_2) \tilde{\rho}_{ss'\mathbf{k}_1} \tilde{\rho}_{s'\mathbf{k}_2} \\ &= \varepsilon_{tot}[|v\mathbf{k}\rangle; \mathcal{E}], \quad (\text{E5}) \end{aligned}$$

which is invariant under the transformation $|v\mathbf{k}\rangle \rightarrow |v'\mathbf{k}\rangle$.

The $U(1)$ symmetry related to exciton conservation (phase ϕ_{ex} of electron-hole pairing condensate $\rho_{eh\mathbf{k}}$) gives a zero energy Goldstone mode to the valance band fluctuation. To see this, let's rewrite $|v'\mathbf{k}\rangle$ into a linear combination of $|v\mathbf{k}\rangle = [\alpha_{\mathbf{k}}, \beta_{\mathbf{k}}]^T$ and $|c\mathbf{k}\rangle = e^{-i\varphi_{\mathbf{k}}} [-\beta_{\mathbf{k}}^*, \alpha_{\mathbf{k}}^*]^T$ ($\varphi_{\mathbf{k}}$ is an arbitrary function of \mathbf{k}) as

$$\begin{aligned} e^{-i\phi} |v'\mathbf{k}\rangle &= \langle v\mathbf{k} | v'\mathbf{k} \rangle |v\mathbf{k}\rangle + \langle c\mathbf{k} | v'\mathbf{k} \rangle |c\mathbf{k}\rangle \\ &= (e^{i\phi_{ex}} |\alpha_{\mathbf{k}}|^2 + e^{-i\phi_{ex}} |\beta_{\mathbf{k}}|^2) |v\mathbf{k}\rangle \\ & \quad - 2i\alpha_{\mathbf{k}} \beta_{\mathbf{k}} \sin \phi_{ex} e^{i\varphi_{\mathbf{k}}} |c\mathbf{k}\rangle \\ &\sim |v\mathbf{k}\rangle - 2i\phi_{ex} \alpha_{\mathbf{k}} \beta_{\mathbf{k}} e^{i\varphi_{\mathbf{k}}} |c\mathbf{k}\rangle, \quad (\text{E6}) \end{aligned}$$

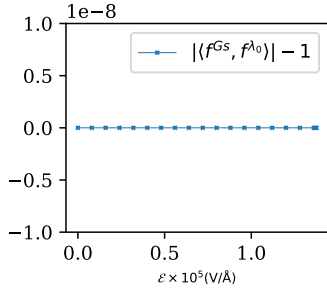


FIG. 5. Overlap between the Goldstone mode Eq. (E7) and the zero mode of the Hessian matrix Eq. (10).

Compare Eq. (D2)(E6) we find the corresponding Gold-

stone mode in parameter space is just expressed as

$$f_{\mathbf{k}}^{Gs} \propto i\alpha_{\mathbf{k}}\beta_{\mathbf{k}}e^{i\varphi_{\mathbf{k}}} = i\langle e|v\mathbf{k};\mathcal{E}\rangle\langle c\mathbf{k};\mathcal{E}|e\rangle. \quad (\text{E7})$$

The overlap between the Goldstone mode $f_{\mathbf{k}}^{Gs}$ and the zero mode $f_{\mathbf{k}}^{\lambda_0}$ of the Hessian matrix Eq. (10) is calculated as

$$I = |\langle f_{\mathbf{k}}^{Gs}, f_{\mathbf{k}}^{\lambda_0} \rangle| = \left| \sum_{\mathbf{k}} (f_{\mathbf{k}}^{Gs})^* f_{\mathbf{k}}^{\lambda_0} \right| \quad (\text{E8})$$

and plotted in Fig. 5. The results show that I is equal to 1 in numerical precision, which means the zero mode of the Hessian matrix is indeed the Goldstone mode $f_{\mathbf{k}}^{Gs}$ discussed in this section.

-
- [1] N. F. Mott, *The Philosophical Magazine: A Journal of Theoretical Experimental and Applied Physics* **6**, 287 (1961).
 - [2] L. V. Keldysh and Y. V. Kopayev, *Soviet Physics Solid State, USSR* **6**, 2219 (1965).
 - [3] D. Jérôme, T. M. Rice, and W. Kohn, *Physical Review* **158**, 462 (1967).
 - [4] B. I. Halperin and T. M. Rice, in *Solid State Physics*, Vol. 21, edited by F. Seitz, D. Turnbull, and H. Ehrenreich (Academic Press, 1968) pp. 115–192.
 - [5] X. Zhu, P. B. Littlewood, M. S. Hybertsen, and T. M. Rice, *Physical Review Letters* **74**, 1633 (1995).
 - [6] L. V. Butov, *Solid State Communications Quantum Phases at the Nanoscale*, **127**, 89 (2003).
 - [7] J. P. Eisenstein and A. H. MacDonald, *Nature* **432**, 691 (2004).
 - [8] L. V. Butov, A. Zrenner, G. Abstreiter, G. Böhm, and G. Weimann, *Physical Review Letters* **73**, 304 (1994).
 - [9] M. M. Fogler, L. V. Butov, and K. S. Novoselov, *Nature Communications* **5**, 4555 (2014).
 - [10] L. Du, X. Li, W. Lou, G. Sullivan, K. Chang, J. Kono, and R.-R. Du, *Nature Communications* **8**, 1971 (2017).
 - [11] J. I. A. Li, T. Taniguchi, K. Watanabe, J. Hone, and C. R. Dean, *Nature Physics* **13**, 751 (2017).
 - [12] Z. Wang, D. A. Rhodes, K. Watanabe, T. Taniguchi, J. C. Hone, J. Shan, and K. F. Mak, *Nature* **574**, 76 (2019).
 - [13] L. Ma, P. X. Nguyen, Z. Wang, Y. Zeng, K. Watanabe, T. Taniguchi, A. H. MacDonald, K. F. Mak, and J. Shan, *Nature* **598**, 585 (2021).
 - [14] Y.-P. Shim and A. H. MacDonald, *Physical Review B* **79**, 235329 (2009).
 - [15] F.-C. Wu, F. Xue, and A. H. MacDonald, *Physical Review B* **92**, 165121 (2015).
 - [16] D. I. Pikulin and T. Hyart, *Physical Review Letters* **112**, 176403 (2014).
 - [17] M. Xie and A. H. MacDonald, *Physical Review Letters* **121**, 067702 (2018).
 - [18] Q. Zhu, M. W.-Y. Tu, Q. Tong, and W. Yao, *Science Advances* **5**, eaau6120 (2019).
 - [19] K. Yang, X. Gao, Y. Wang, T. Zhang, P. Gu, Z. Luo, R. Zheng, S. Cao, H. Wang, X. Sun, K. Watanabe, T. Taniguchi, X. Li, J. Zhang, X. Dai, J. Chen, Y. Ye, and Z. V. Han, *Realization of graphene logics in an exciton-enhanced insulating phase* (2021), arXiv:2110.02921 [cond-mat].
 - [20] N. Sugimoto, S. Onoda, and N. Nagaosa, *Physical Review B* **78**, 155104 (2008).
 - [21] G. Nenciu, *Reviews of Modern Physics* **63**, 91 (1991).
 - [22] I. Souza, J. Íñiguez, and D. Vanderbilt, *Physical Review Letters* **89**, 117602 (2002).
 - [23] C. Zener and R. H. Fowler, *Proceedings of the Royal Society of London. Series A, Containing Papers of a Mathematical and Physical Character* **145**, 523 (1934).
 - [24] G. H. Wannier, *Physical Review* **117**, 432 (1960).
 - [25] E. O. Kane, *Journal of Physics and Chemistry of Solids* **12**, 181 (1960).
 - [26] R. Resta, *Physical Review Letters* **80**, 1800 (1998).
 - [27] J. Zak, *Physical Review Letters* **62**, 2747 (1989).
 - [28] D. Vanderbilt and R. D. King-Smith, *Physical Review B* **48**, 4442 (1993).
 - [29] R. D. King-Smith and D. Vanderbilt, *Physical Review B* **47**, 1651 (1993).
 - [30] R. W. Nunes and X. Gonze, *Physical Review B* **63**, 155107 (2001).
 - [31] J. Íñiguez, D. Vanderbilt, and L. Bellaiche, *Physical Review B* **67**, 224107 (2003).
 - [32] R. W. Nunes and D. Vanderbilt, *Physical Review Letters* **73**, 712 (1994).
 - [33] P. Fernández, A. Dal Corso, and A. Baldereschi, *Physical Review B* **58**, R7480 (1998).